Materials Characterization 205 (2023) 113252

Contents lists available at ScienceDirect

Materials Characterization

journal homepage: www.elsevier.com/locate/matchar

# Microstructure evolution and texture development during production of homogeneous fine-grained aluminum wire by friction extrusion

Uceu F.H. Suhuddin [a,*], Lars Rath [a], Ricardo M. Halak [b], Benjamin Klusemann [a,b]

[a] Solid State Materials Processing, Institute of Materials Mechanics, Helmholtz-Zentrum Hereon, Max-Planck-Str. 1, 21502 Geesthacht, Germany
[b] Institute for Production Technology and Systems, Leuphana University Lüneburg, Universitätsallee 1, 21335 Lüneburg, Germany

ARTICLE INFO

*Keywords:*
Friction extrusion
Dynamic recrystallization
Simple shear texture
Material flow
Aluminum alloy

ABSTRACT

This study aims to understand the microstructure evolution and texture development during friction extrusion of aluminum alloys, focusing on AA7075 as exemplary alloy system. Electron backscatter diffraction technique has been employed to obtain crystallographic data from various regions in front of the die and in the wire. It can be deduced that the combination of continuous dynamic recrystallization and geometric dynamic recrystallization mainly govern the formation of a fine-grained structure, however discontinuous dynamic recrystallization may also play a role at high temperature. The global shear deformation during the process was characterized as a simple shear deformation with dominant $B/\overline{B}$ simple shear texture components. The material flow is mainly driven by the in-plane shear strain and the extrusion-induced shear strain that are determined by die rotational speed and extrusion force, respectively. The in-plane shear strain strongly affects the formation of a homogeneous fine-grained microstructure in the aluminum wire. In this regard, a novel material flow model for friction extrusion has been proposed.

## 1. Introduction

Friction Extrusion (FE) is a friction-based process capable of producing advanced material in different shapes, such as wire, rod and hollow structures. FE has the same principle as friction stir welding/processing (FSW/P), utilizing a non-consumable tool to introduce severe plastic deformation and to generate frictional heat for material consolidation. FE is able to process materials in different forms of solid materials [1–4], chips [5–7] and powder [8]. Fig. 1 presents a schematic illustration of the general FE process for wire production. A non-consumable die starts to rotate and presses against the material to be processed. The rotating die plastically deforms the material and generates frictional heat that softens the material. Then, it extrudes the plasticized material through the die orifice, forming a consolidated wire.

FE is characterized as an energy efficient process since it requires no external heating and relatively low extrusion force to produce high quality extrudate [2,9]. FE is potentially used to produce advanced materials with enhanced properties, i.e. lightweight materials with superior mechanical properties [2,3] and electrical conductivity [10]. Additionally, the ability to extrude metal chips and swarf [6,11–13], i.e. recycling machining waste, classifies this process as sustainable and environmentally friendly.

Some studies have been carried out to produce advanced aluminum (Al) wires by FE from bulk materials [1–4], machining chips [5–7] and powder [8]. Utilization of a 90° scroll die [1,2,4,6] or a 60° featureless die [3] in FE of bulk Al alloys has proven to fabricate wires with homogeneous fine-grained structure and uniformly distributed secondary particles. It is believed that dynamic recrystallization, which commonly occurs in Al alloys during thermo-mechanical processing, is responsible for the grain refinement during FE [1–3,14]. Additionally, Li et al. [4] showed that static recrystallization occurred after the material passed through the die. Nevertheless, formation and development of the recrystallized grain structure during FE, i.e. in front of the die, remains unclear.

Halak et al. [3] and Li et al. [4] showed that alteration of the heat input during FE process, i.e. high processing temperatures, affects the process stability, which turned the homogeneous to an inhomogeneous microstructure wire. In an attempt to understand the microstructure evolution during FE, some studies have been carried out using marker materials inserted in the base material (BM) [4,15]. The distribution and grain characteristic of the marker materials were characterized in the extruded wires. It was mentioned that presence of the longitudinal strain

* Corresponding author.
*E-mail address:* uceu.suhuddin@hereon.de (U.F.H. Suhuddin).

https://doi.org/10.1016/j.matchar.2023.113252
Received 24 March 2023; Received in revised form 3 July 2023; Accepted 17 August 2023
Available online 19 August 2023
1044-5803/© 2023 The Authors. Published by Elsevier Inc. This is an open access article under the CC BY license (http://creativecommons.org/licenses/by/4.0/).

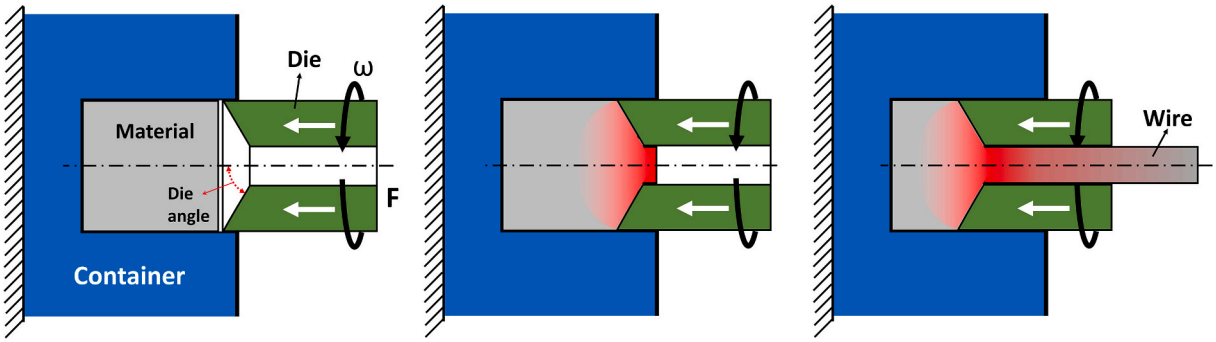


**Fig. 1.** A schematic illustration of the Friction Extrusion process.

and in-plane shear strain plays an important role in the formation of a homogenous fine-grained structure, in addition to the processing temperature. When the heat input is too high, the in-plane shear strain decreases, where FE becomes similar to conventional extrusion [3,4]. Nonetheless, the material flow behavior concerning development of shear deformation resulted in a homogenous fine-grained structure during FE needs more clarification.

There are three typical dynamic recrystallization mechanisms introduced in metallic materials during thermomechanical processing, which are continuous dynamic recrystallization (CDRX), geometric dynamic recrystallization (GDRX) and discontinuous dynamic recrystallization (DDRX) [16,17]. Formation of the recrystallized grain structure by CDRX includes transformation of low angle grain boundaries (LAGBs) to high angle grain boundaries (HAGBs) due to the accumulation of dislocations [17–21]. In GDRX, the recrystallized grain structure is formed by pinching off the highly deformed initial grains due to geometrical effect of strain [17,19,21,22]. In DDRX, the recrystallized grain structure appears at the initial grain boundaries which has clear nucleation and growth [20,23,24]. CDRX and GDRX are typically reported for materials with high stacking fault energy, while DDRX is more typical for low stacking fault energy materials [16]. Al alloy is one of the metallic alloys that has high stacking fault energies, in which dynamic recovery through dislocation climb is dominant. However in addition to CDRX and GDRX, DDRX has also been observed in Al alloys during thermomechanical processing [17–22]. In this study, grain refinement mechanism in an Al alloy during FE process with regards to recrystallization mechanism will be studied.

In the present study, FE is applied to produce defect-free wires from bulk AA7075 using a 60° featureless die. The microstructure and texture evolution during FE were systematically investigated to establish a basic understanding of the formation of a homogeneous fine-grained microstructure and the material flow during FE.

## 2. Experimental procedure

The material used in the present study was aluminum alloy 7075 in T651 temper (AA7075-T651). It has main alloying elements of 5.8 wt% Zn, 2.3 wt% Mg and 2.0 wt% Fe. The AA7075-T651 rolled plate was cut into dimension of 200x200x30 $mm^3$. Two plates of the AA7075 were stacked on top of each other and heated up to 40 °C prior to the FE process to maintain identical starting condition. The AA7075-T651 sheet was friction-extruded in a bead-on-plate configuration, i.e. extrusion direction (ED) aligned with normal direction (ND) of the sheet. The experimental setup is presented in detail in the previous study of the authors [3].

The FE process was carried out on a customized friction-surfacing machine (RAS), manufactured by Henry Loitz Robotik, Germany. The non-consumable die used in this study was made of AISI H13 steel. The 60° die has no feature on its surface with 15 mm outer diameter and 6 mm inner diameter, which leads to an extrusion ratio (ER) of 6.25. The process was performed force-controlled at a constant rotation speed of 300 rpm and extrusion forces (F) between 16 and 22 kN. No significant flash was formed in the Al sheet around the outer side of the die during FE because the die forced the material into the conical die. Since the FE is performed using a constant extrusion force, the extrusion rate may vary during the process, as discussed in detail by Halak et al. [3].

For microstructure analysis, the samples were sectioned, ground and polished in colloidal silica, according to standard metallographic sample preparation. The samples were electrically etched with Barker's solution and analyzed using a Keyence VHX-600 digital microscope and a Leica DMi8 optical microscope (OM) under polarized light. Further microstructure analysis was performed using an FEI Quanta 650 field emission gun (FEG) scanning electron microscope (SEM) equipped with a TSL OIM electron backscatter diffraction (EBSD) system and an EDAX energy dispersive X-ray spectroscopy (EDS) system.

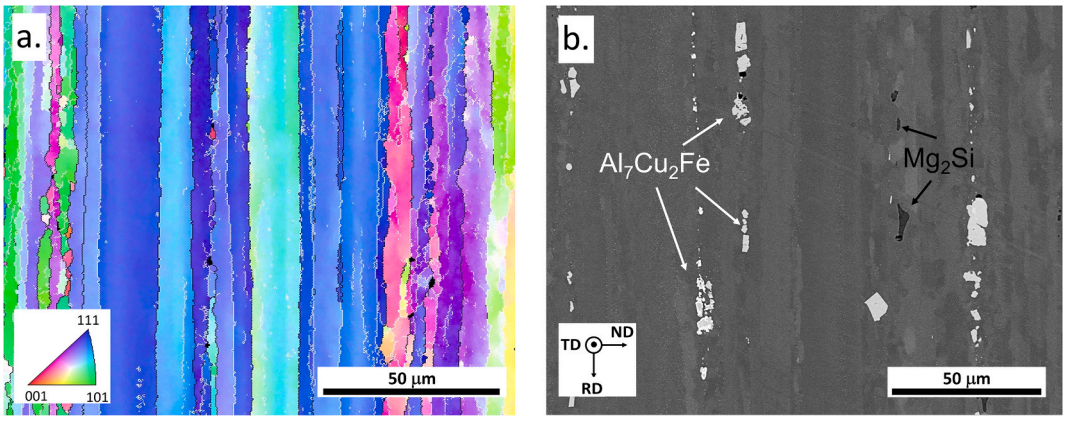


**Fig. 2.** Microstructure of the rolled AA7075-T651 base material, IPF map (a) and backscatter image (b).


**Fig. 3.** Macrographs and micrographs of the extruded wires produced by a rotation speed of 300 rpm, extrusion forces lower (a) and higher (b) than 19 kN, i.e. 16 kN and 20 kN, respectively.

Orientation mapping was performed with a step scan of 0.3 μm. A lower limit boundary misorientation cut-off of 2° was used to eliminate spurious boundaries. The obtained crystallographic data is expressed as inverse pole figure (IPF) map, misorientation-angle distribution, pole figure (PF) and orientation distribution function (ODF). The 15° criterion was used to define LAGBs and HAGBs. All ODFs are sectioned from Euler angle, $\phi_2$=0° and 45°.

## 3. Results and discussion

### 3.1. Base material

The microstructure features of the AA7075 rolled plate are summarized in Fig. 2. The microstructure consists of mainly large elongated grains and small amount of fine grains in between the large grains, with

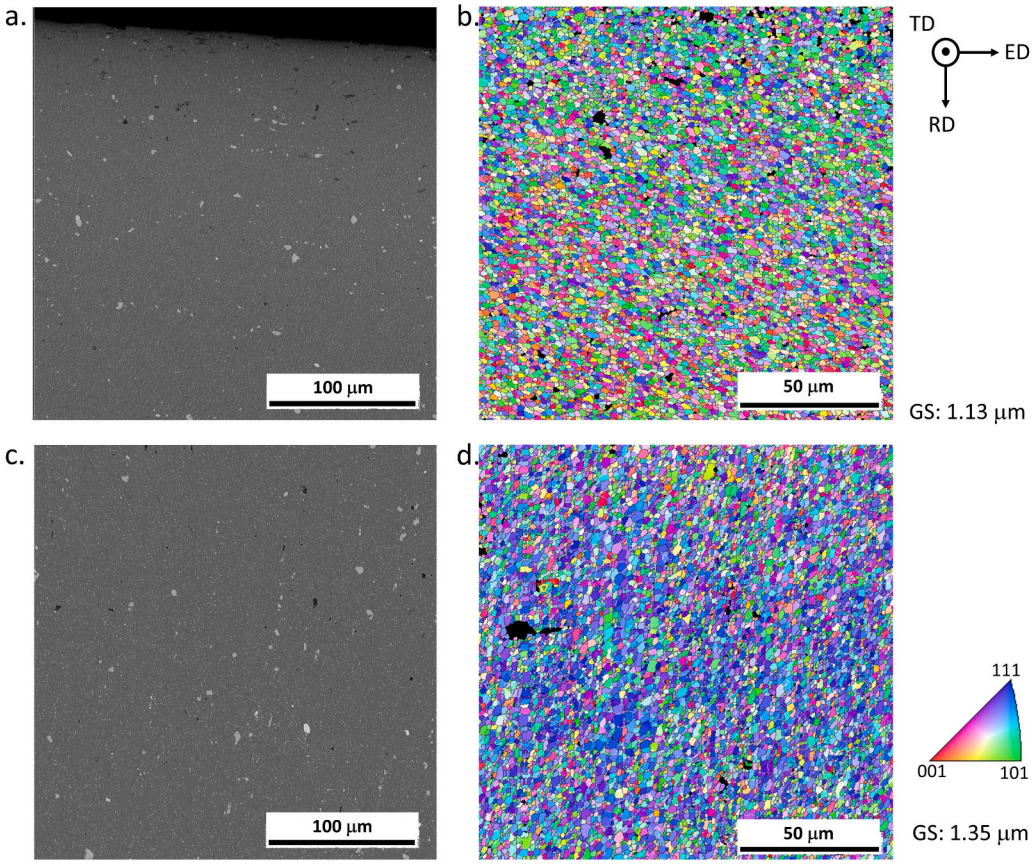


**Fig. 4.** Backscatter electron images and IPF maps of the homogeneous fine-grained wire acquired from the outer diameter (a, b) and center of the wire (c, d), produced at 20 kN and 300 rpm. The dark and bright particles (in a and c) are $Mg_2Si$ and $Al_7Cu_2Fe$, respectively.

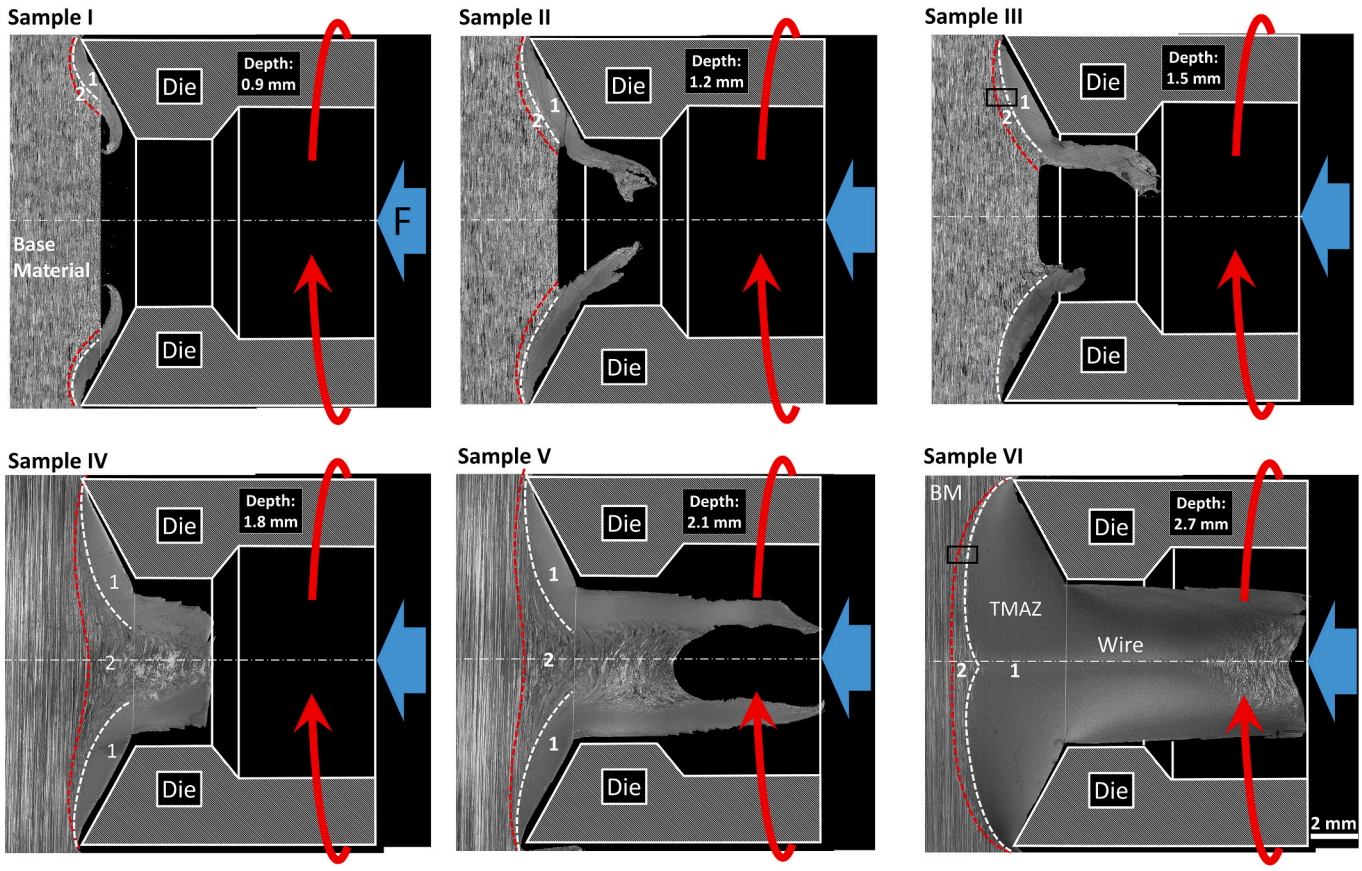


**Fig. 5.** Serial FE processes (20 kN, 300 rpm) applied to AA7075 sheet up to several plunge depths of 0.9, 1.2, 1.5, 1.8, 2.1 and 2.7 mm.

an average thickness of about 7 μm. EDS characterization shows that bright/dark particles in the backscatter image are identified as secondary particles of $Mg_2Si$ (dark particles) and $Al_7Cu_2Fe$ (bright particles), which align along the rolling direction (RD). The rolling texture is dominated by Brass {110} ⟨112⟩ and S {123} <634> as well as Cube {100}⟨001⟩ and S1 {214} ⟨121⟩ texture components.

### 3.2. Macrostructure of the wires

Fig. 3 presents the surface appearances as well as macrographs in the longitudinal- and cross-section of the wires fabricated by extrusion forces lower and higher than 19 kN. The wires have a nominal diameter of 6 mm and length between 75 and 80 mm. No defects such as voids are visible in the wires. The wire produced by an extrusion force lower than 19 kN has an inhomogeneous microstructure with a fine-grained structure in the outer region and an elongated grain structure in the inner region, Fig. 3a. On the other hand, the wire produced by an extrusion force higher than 19 kN consists of a homogeneous fine-grained structure, Fig. 3b.

The wires have tool marks on the surfaces in which its pitch distance can be calculated as the extrusion speed divided by the rotation speed. As mentioned by Halak et al. [3], the maximum calculated pitch-distance of a wire produced by 300 rpm at resulting extrusion speeds up to 2.96 mm/s is about 0.592 mm. For further details on the processing characteristics during the FE experiments, such as die advancing rate or temperature evolution, the interested reader is referred to Halak et al. [3]. Observations of the surface pattern on the wire show a good agreement with the calculated pitch-distance of the wires produced by an extrusion force lower than 19 kN. However, the wires produced with the extrusion force higher than 19 kN have much larger pitch distances than the calculated value, i.e. 220 mm or even larger [3], as shown in Fig. 3b. This result indicates that the relative rotation between the rotating die and the wire for extrusion forces >19 kN is relatively low or nearly zero.

### 3.3. Microstructure evolution

The focus of the current study is the understanding of the microstructure formation and material flow in homogeneous fine-grained wires, which will be discussed in more detail in the following. Microstructure in a cross-section of the wire extruded at 20 kN extrusion force is presented in Fig. 4, captured from the outer diameter and center of the wire. The microstructure comprises fine-equiaxed grains with an average diameter of about 1.2 μm. It is also clearly seen that the large $Mg_2Si$ and $Al_7Cu_2Fe$ particles observed in the BM are fragmented into smaller particles and randomly distributed in the wire.

To get a better understanding of microstructure evolution and material flow, FE processes have been applied until several die plunge depths between 0.9 and 2.7 mm, see Fig. 5. As soon as the rotating die reached the pre-defined depth, it was retracted immediately to avoid further deformation and heat exposure to the samples. No external cooling has been applied to the material following the FE process, i.e. heat dissipated mainly to the bulk Al base materials and FE machine. During metallographic sample preparation, flashes in wire tips of some samples were broken off, resulting in irregular shapes.

Based on the grain characteristic, some microstructural zones in front of the die orifice can be identified, namely the unaffected BM, a thermo-mechanically affected zone (TMAZ) 1 that comprises a fine-grained structure and a TMAZ 2 that consists of a deformed grain structure, see for instance Sample VI in Fig. 5. After the die orifice, i.e. the smallest die diameter where extrusion starts, the region is simply referred to as wire in the following.

At the beginning of the process, introduction of plastic deformation and high thermal exposure during die plunging leads to formation of a

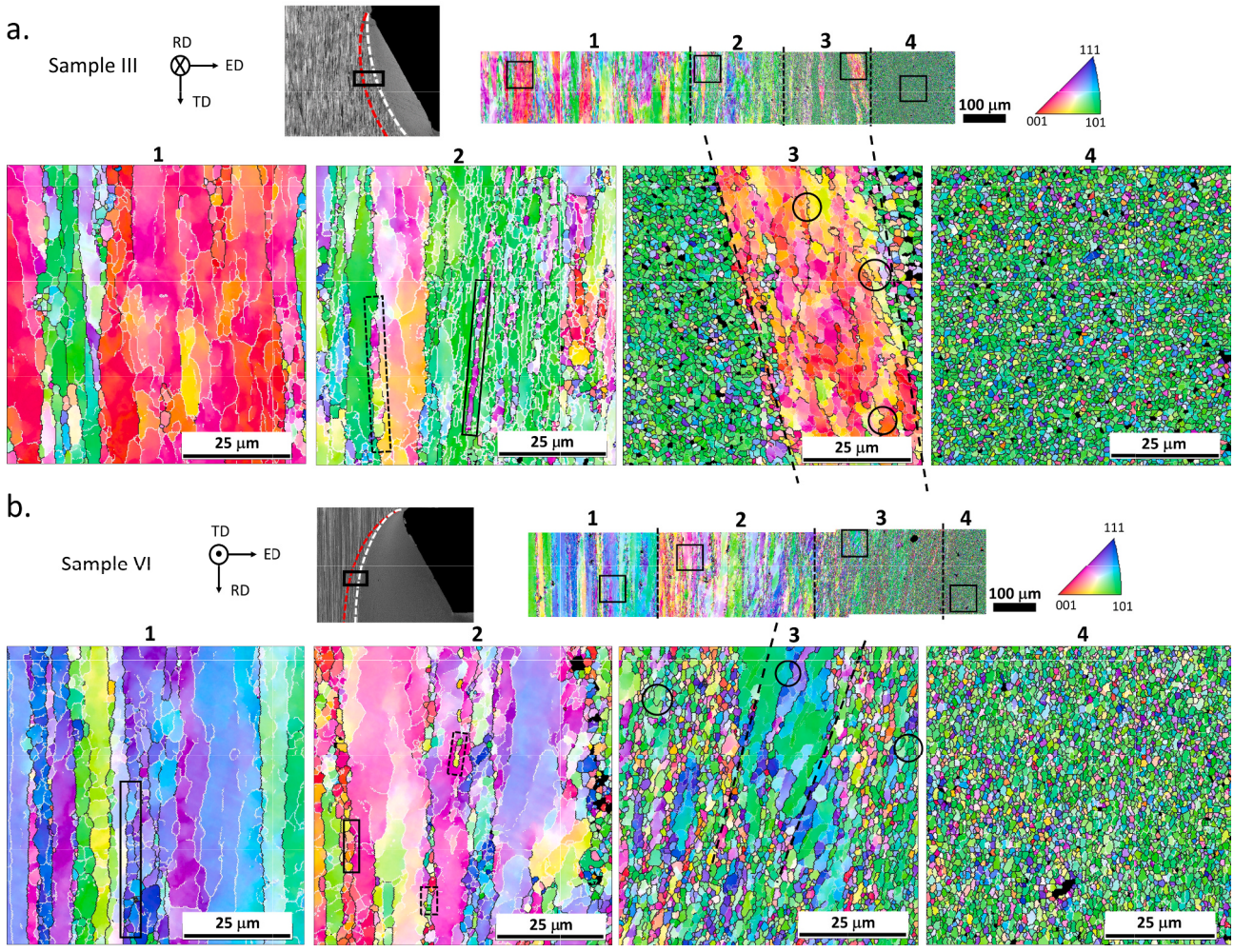


**Fig. 6.** EBSD maps taken from the transition regions in Sample III (a) and Sample VI (b). The grain refinement by subdivision of elongated grains and sub grain rotation are highlighted by the solid and dash rectangles in the EBSD maps at higher magnification, respectively. Bulging along the grain boundaries is highlighted by dark circulars. LAGBs and HABGs are depicted as white and black lines in the IPF maps, respectively.

fine-grained structure (TMAZ 1) near the contact area between the material and the rotating die at the outer diameter. Then, the fine-grained structure flows along the die surface towards the die orifice as the plunge depth increases, as depicted for Samples I-V in Fig. 5. After the fine grains reach the centerline in front of the die orifice, they build up towards the BM forming a large TMAZ 1, as shown in Sample VI. Finally, the fine-grained structure in TMAZ 1 is extruded through the die orifice, resulting in a consolidated wire with homogeneous fine-grained microstructure. At the same time, the TMAZ 2, which consists of a deformed grain structure, is also formed and develops accordingly in between the TMAZ 1 and BM. However, deformation and temperature in TMAZ2 are not high enough to induce recrystallization.

### 3.3.1. *Microstructure evolution in transition zone*

To understand the microstructure evolution during FE, large EBSD maps were acquired from the transition regions in Sample III and Sample VI, as depicted in Fig. 6. Based on the microstructural features, the EBSD maps are divided into four regions. The grain size, which is translated in terms of HAGB spacing in ED and HAGB fraction extracted from the regions, is summarized in Table 1.

In regions 1 and 2, formation of LAGBs inside the large grain interior is clearly observed due to dislocation accumulation induced by the shear strain. Continuous absorption of the dislocations in the grain boundaries leads to an increase in the misorientation angle. Some of the LAGBs transform into HAGBs when the grain misorientation exceeds 15°

**Table 1**
HAGB spacing in ED extracted from several regions in transition area.

| Region | HAGB spacing in ED (μm) | |
|---|---|---|
| | Sample III | Sample VI |
| BM | 7.16 | 7.16 |
| Region 1 | 4.49 | 6.32 |
| Region 2 | 2.66 | 2.98 |
| Region 3 | 1.02 | 1.03 |
| Region 4 | 0.84 | 0.84 |

dividing the large grains into smaller grains. It is also seen that the thickness of some elongated grains decreases due to geometrical requirement of strain. An increase in the strain induces progressive lattice rotation and grain subdivision, which transforms the thin elongated grains into new fine-recrystallized grains, indicating CDRX, as presented in Fig. 7a. As the temperature increases, the grain boundaries become serrated. The thin elongated grain was pinched off into fine grains, indicating GDRX, as presented in Fig. 7b. Comparing both mechanisms, the orientation of the lattice-rotated sub-grains in CDRX change through grain boundary rotation, while the orientation of the pinched-off sub-grains remains in GDRX consistent with their initial grains. Formation of the fine grains decreases the HAGB spacing in the regions 1 and 2, as presented in Table 1. Grain refinement induced by accumulation of grain misorientation angle in Al alloys during thermo-

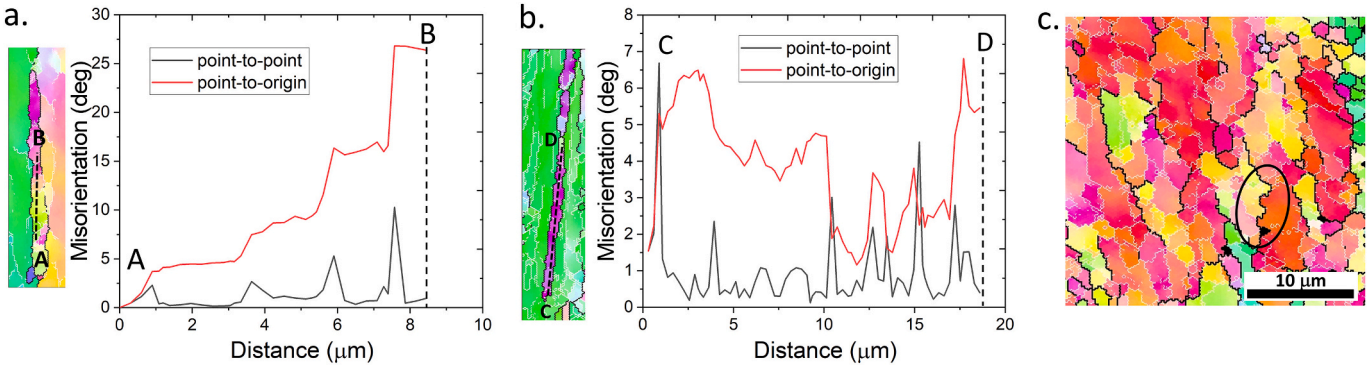


**Fig. 7.** Distribution of misorientation angle along the elongated grains experiencing sub-grain rotation (a) and without sub-grain rotation (b) taken from Region 2. (c) An example of grain boundary bulging induced by local boundary migration taken from Region 3 in sample 3, as shown in Fig. 6.

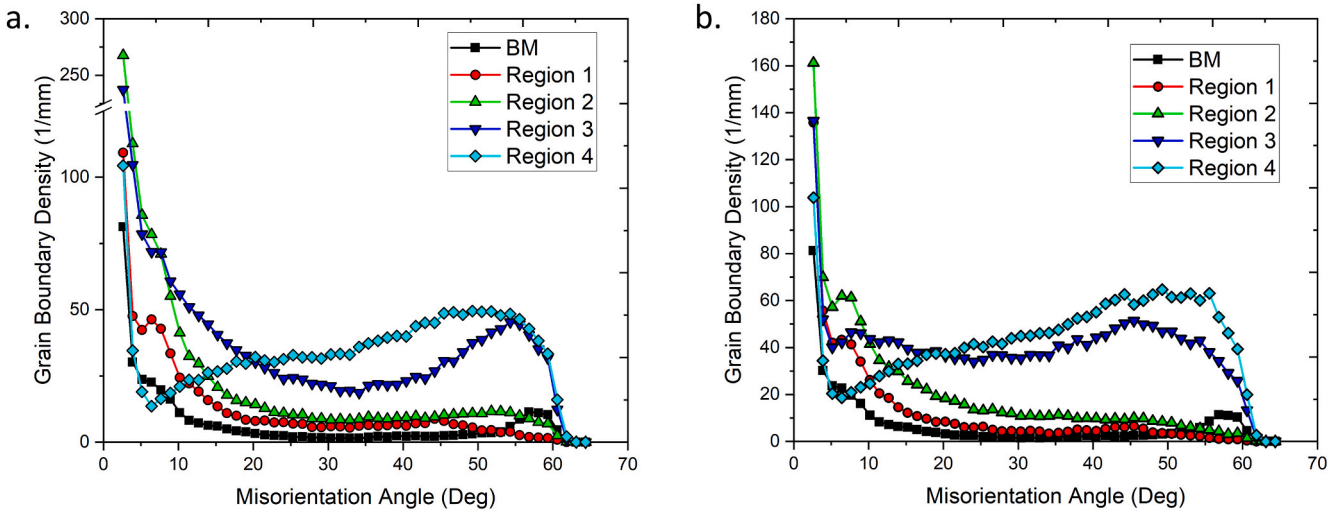


**Fig. 8.** Grain boundary densities extracted from several regions in Samples III (a) and Sample VI (b), taken from the transition region between TMAZ and BM in these samples, see Fig. 6.

mechanical processing has been well-documented [18–20,23,24].

In the area closer to the die, Region 3 has a bi-modal structure consisting of a fine-equiaxed and a large-deformed grain structure, as depicted in Fig. 6 for both samples. The large-deformed grain structure experienced further grain subdivision induced by misorientation angle accumulation and geometric effect of strain, indicating further CDRX and GDRX, respectively. As the temperature during the FE process increases, the grain boundaries become wavy, indicating local grain boundary migration. The local migration generates bulging along the grain boundaries, see Fig. 7c, which then transform into fine grains or experiencing DDRX. Ultimately, the large-deformed grains transform into a fine-grained structure as shown in Region 4. The homogenous fine-grained structures have an average grain size of <1 μm with strong grain orientation of ⟨110⟩ perpendicular to observation plane.

In order to compare directly the grain boundaries between different microstructural regions, the misorientation-angle data are asserted in terms of specific grain boundary length or grain boundary density, which is calculated as the grain boundary length in the region of interest divided by the area of the corresponding region. Fig. 8 displays the grain boundary densities obtained from regions 1–4 in samples III and VI. Formation of extensive deformation-induced grain boundaries with subsequence accumulation of misorientation angles leads to increase the HAGBs and LAGBs significantly in regions 1 and 2. Formation of grain boundaries marked by progressive movement of the long-angle peak towards high-angle misorientation induced by accumulation of misorientation angle or CDRX [18,21,25] primarily governs the grain structure in the regions. Additionally, formation of fine grain structure induced by geometric effect of strain without sub-grain rotation or GDRX [20,23,24] seems to give a contribution to development of the HAGBs. Meanwhile, a decrease of LAGBs coupled with major formation of HAGBs in regions 3 and 4 at misorientation angle larger than 30°, is most likely associated with the observed GDRX and grain-boundary bulging or DDRX, as well as CDRX. Elimination of the LAGBs in these regions is associated with grain boundary migration as well as transformation of existing LAGBs to HAGBs. Therefore, the grain refinement in this region should be mainly determined by GDRX and CDRX with limited DDRX [20,23,26,27]. Since AA7075 is a precipitation hardening Al alloys, the presence of high densities of several types of fine precipitates and particles in this alloy might act as obstacles for the dislocation movement, preventing recrystallization [28]. Considering the processing temperature during FE is typically higher than 450 °C [2], most of the strengthening precipitates should be dissolved in the Al matrix, reducing the resistance against dislocation movement towards the grain boundaries. Dislocation motion as well as grain boundary sliding promote boundary migration, followed by subgrain rotation, giving rise to the development of new recrystallized grains [18,24,25].

Grain refinement driven by CDRX, GDRX and additionally DDRX at elevated temperature in high stacking fault energy materials such as Al

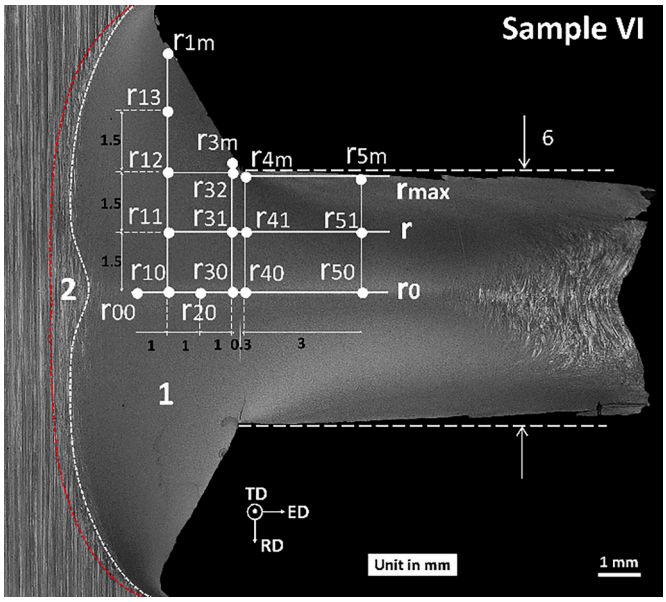


**Fig. 9.** Map of EBSD scanned area in the TMAZ 1 and wire of Sample VI. Regions r4 (including r40, r41 and r4m) represents the TMAZ 1 – wire transition line. Numbers in black color indicate the distance between the scanned area in mm.

alloys, has been reported during thermo-mechanical processing [18–20,23–27]. Therefore, the microstructural evolution is dependent on the temperature and strain rate in addition to the strain during thermo-mechanical processing, which can be described using the Zener-Hollomon parameter

$$Z = \dot{\varepsilon}\, expQ/RT \quad (1)$$

where $\dot{\varepsilon}$ is the strain rate, Q is the activation energy, R is the universal gas constant and T is the processing temperature. When the temperature gradually increases, i.e. material is approaching the die surface, the Z value decreases accordingly, which then transforms the recrystallization mechanism in Al alloys from CDRX to GDRX and DDRX, as also reported in previous studies [17,18,29,30]. It is important to note that the contribution of the recrystallization types should depend on the specific FE parameters, determining the introduced shear strain and heat input.

### 3.3.2. Development of microstructure in TMAZ 1 and the wire

To understand the microstructure evolution in the TMAZ 1 during the FE process and in the wire, EBSD data have been acquired from various regions, as presented in Fig. 9. It is important to note that the diameter of wire attached to the TMAZ 1 is the same as the die inner diameter, while the final wire diameter is about 0.3 mm smaller. During die retraction after FE, the wire end experienced additional deformation from the die orifice; thus, the region r4m is excluded in the following microstructure study.

Fig. 10 presents the microstructure taken from several regions along the centerline of the material (radius, $r = 0$) in TMAZ 1 and wire. All regions comprise fine-recrystallized grains with strong crystallographic orientations ⟨111⟩ parallel to TD. The grain size slightly increases from 1.39 μm at an area near the BM (r00) to 1.54 μm at the die orifice (r40), which might be associated with grain growth. Then it decreases down to 1.35 μm in the extruded wire (r50), indicating alteration of strain condition.

Fig. 11 illustrates the IPF maps obtained from various regions at different distances to the centerline, i.e. $r > 0$. Most of the area consists of fine grains with a strong crystallographic orientation of ⟨101⟩ parallel

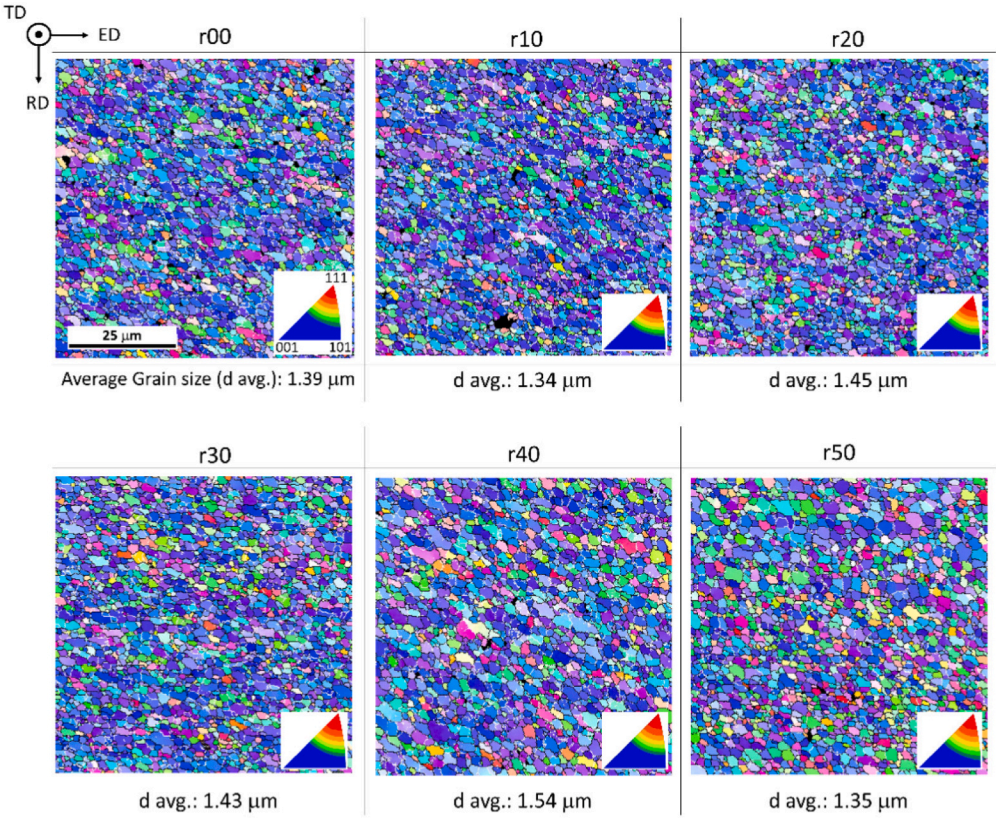


**Fig. 10.** IPF maps obtained from several regions along the centerline of TMAZ 1 and extruded wire of Sample VI. The locations correspond to Fig. 9.

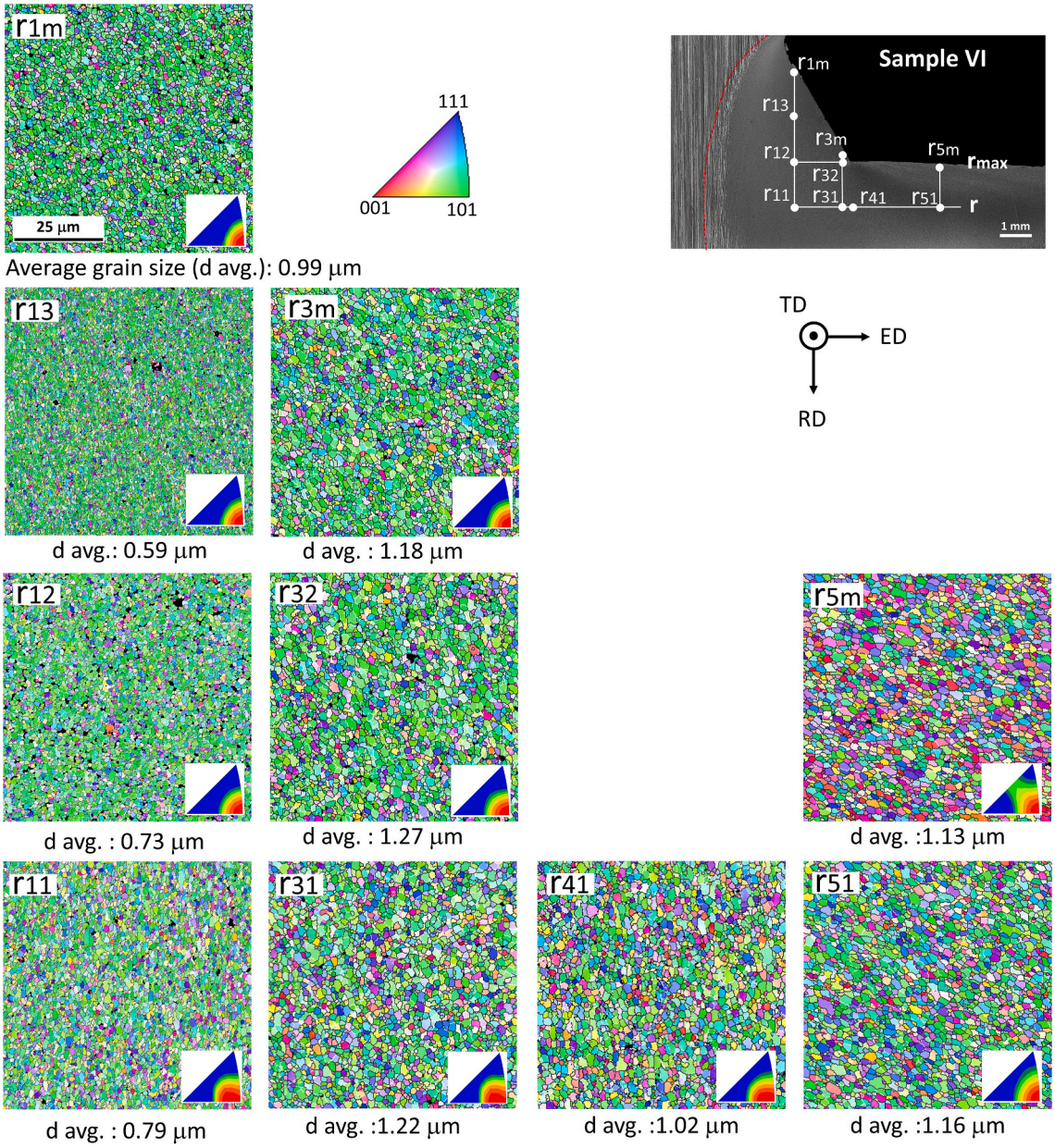


**Fig. 11.** IPF maps obtained from several regions of Sample VI within TMAZ 1 and extruded wire at $r > 0$, according Fig. 9.

to TD, which is different with those in the regions along the centerline ($r = 0$). A new grain orientation in between ⟨100⟩ and ⟨111⟩ poles in region r5m, i.e. near the outer radius of the wire, indicates alteration of strain when passing the die orifice.

In general, the grain size becomes smaller towards the outer radius and larger towards the wire in TMAZ 1. Variation in the grain size corresponds to the degree of shear deformation and temperature exposure in each region during FE, i.e. deformation becomes larger with increasing radius, while the temperature increases towards the die. Due to high temperature exposure, grain growth occurred within the microstructure. Finally, the material is subjected to additional deformation during extrusion at the die orifice, leading to a further refinement.

## 4. Development of texture during FE process

FE is a thermo-mechanical processing technology, involving severe strain, high temperatures and high strain rates, which makes this process broadly similar to other processes, such as conventional extrusion process, FSW/P and high-pressure torsion (HPT) [19,20,23,25,29,31–33]. Therefore, in terms of the following texture analysis, the deformation state and the material flow in this study is considered in the context of the behavior reported for the mentioned processes.

To understand the material flow during FE, the orientation data was derived from the transition region and arranged as 111 and 110 PFs. An appropriate coordinate reference needs to be established to recognize the observed textures and to reveal the actual physical process, i.e. material flow. The predominant deformation mode in FE is expected to be close to simple shear texture, which is defined in terms of crystallographic plane and direction aligned with the shear plane (SP) and shear direction (SD), respectively.

The 111 and 110 PFs obtained from various regions in the TMAZ 1 and the wire, according to Fig. 8, are presented in Fig. 12. At the regions along the outer radius in front of the die (r1m and r3m), the PFs have similar texture components with intensity peaks in the upper and lower poles deviating counterclockwise (CCW) from the vertical line. During

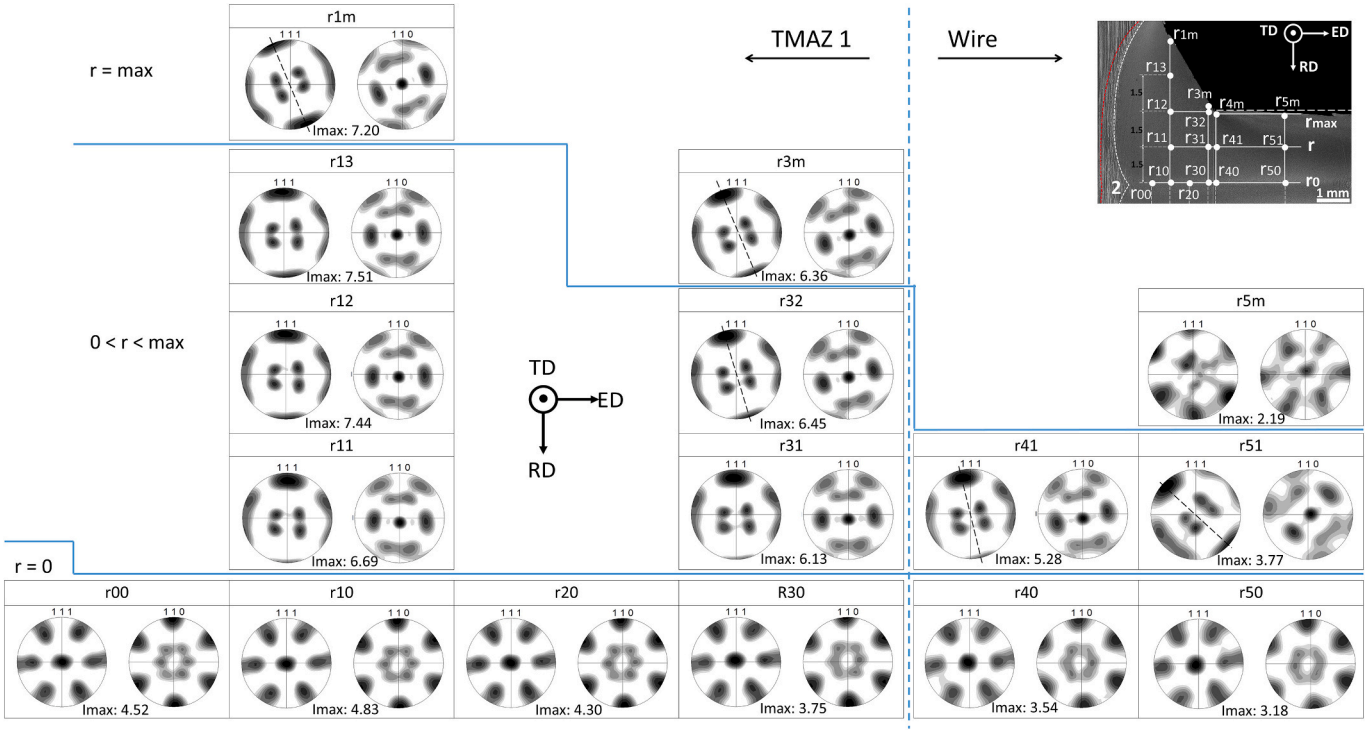


**Fig. 12.** Pole figure maps obtained from various regions of Sample VI within TMAZ 1 and extruded wire, according to Fig. 9. Imax is the maximum texture intensity in multiples of a random distribution (mrd) unit.

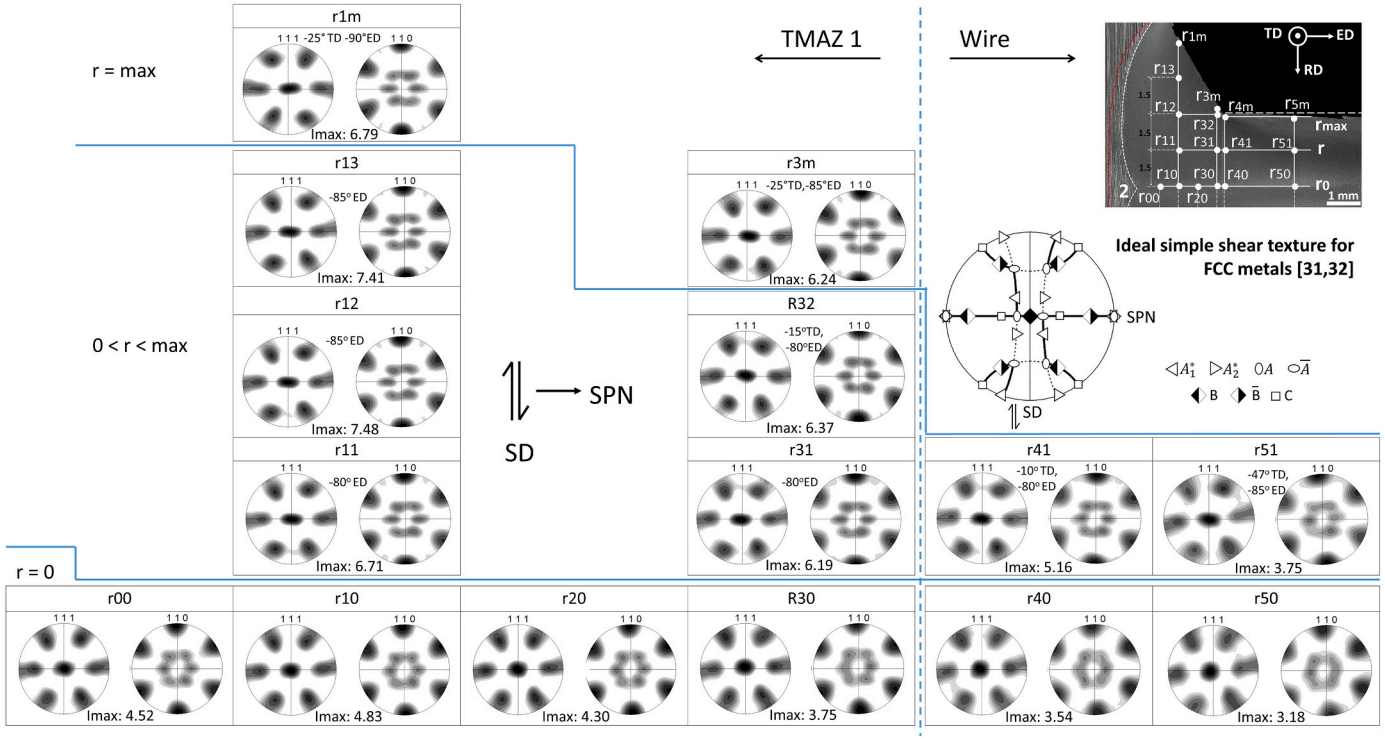


**Fig. 13.** As-rotated pole figures from Fig. 12 to align SPN horizontal and SD vertical. Imax is the maximum texture intensity in multiples of a random distribution (mrd) unit.

FE, the rotating die presses against the material and shears the imminent material. Therefore, it is reasonable to assume that the SP in these regions aligns parallel to the die face, i.e. about −30° from the vertical line. Rearrangement of the as-acquired PFs to align the shear plane normal (SPN) horizontally and SD vertically shows that the PFs can be interpreted as a strong $B/\overline{B}$ {112} <110> including weak $A_1^*/A_2^*$ {111}⟨112⟩ and C {100}⟨110⟩ shear texture components, as shown in Figs. 13 and 14.

As-acquired 111 and 110 PFs obtained from several regions along the

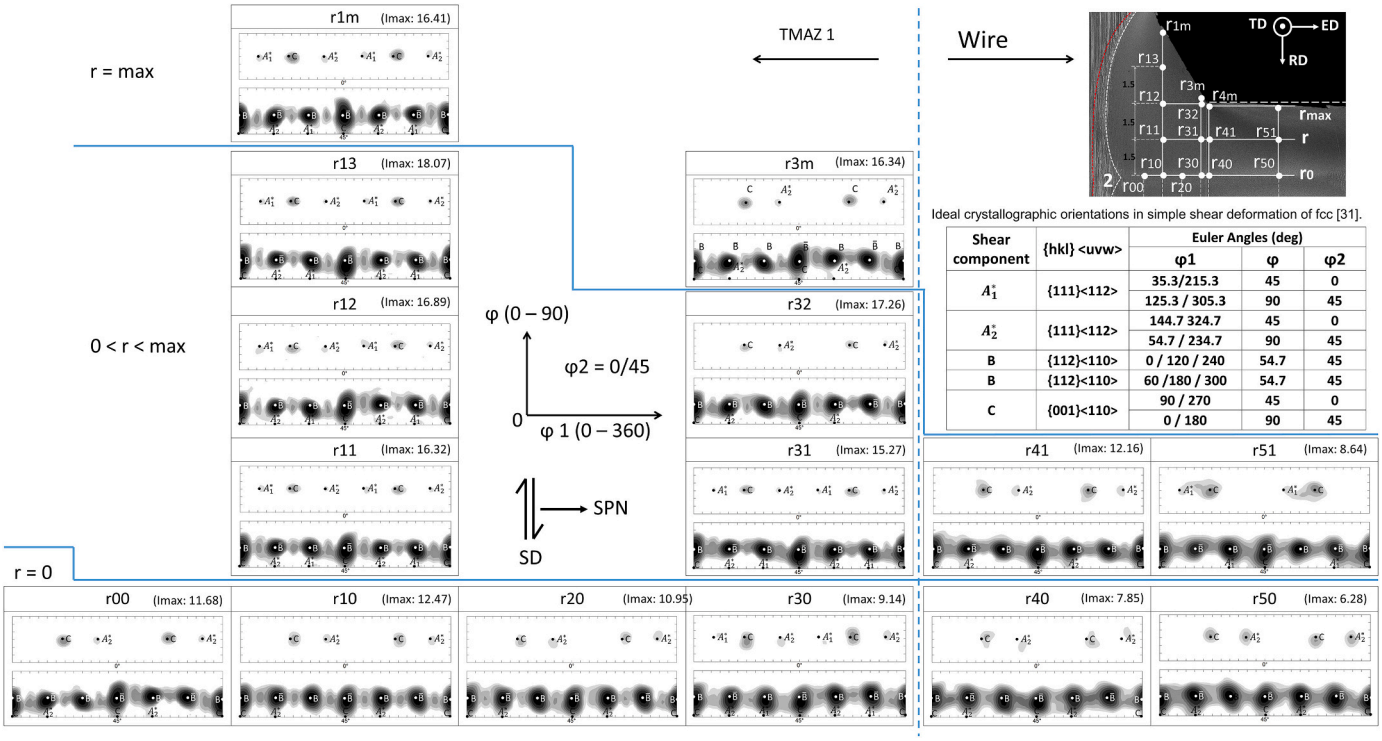


Ideal crystallographic orientations in simple shear deformation of fcc [31].

| Shear component | {hkl} <uvw> | Euler Angles (deg) | | |
|---|---|---|---|---|
| | | φ1 | φ | φ2 |
| $A_1^*$ | {111}<112> | 35.3/215.3 | 45 | 0 |
| | | 125.3 / 305.3 | 90 | 45 |
| $A_2^*$ | {111}<112> | 144.7 324.7 | 45 | 0 |
| | | 54.7 / 234.7 | 90 | 45 |
| B | {112}<110> | 0 / 120 / 240 | 54.7 | 45 |
| B | {112}<110> | 60 /180 / 300 | 54.7 | 45 |
| C | {001}<110> | 90 / 270 | 45 | 0 |
| | | 0 / 180 | 90 | 45 |

**Fig. 14.** Orientation distribution function maps of pole figures in Fig. 13. Imax is the maximum texture intensity in multiples of a random distribution (mrd) unit.

radius (0 < r < r max) in the TMAZ 1 have identical texture components with strong <101> parallel to TD, except small deviation in region r32, as shown in Fig. 12. The PFs have the same texture components with those in the regions r1m and r3m, indicating a simple shear texture with some deviations. Meanwhile, the PFs along the centerline ($r = 0$) in TMAZ 1 have identical texture components with strong <111> parallel to TD. All investigated regions within the TMAZ 1 (except the outer regions, r max) are expected to experience less die-face-induced shear strain because their locations are still away from the die. Based on the loading direction, the deformation state in these regions seems to be comparable to that in HPT [33,34], in which the tool compression is applied perpendicular to the material surface. It is well-established that the predominant deformation in HPT is simple shear with the SPN and SD aligned and tangential to the rotation axis, respectively [33,34]. Based on this approximation, the as-acquired PFs in regions along the radius, 0 < r < r max, should be rotated 90° around the ED and no rotation is necessary in regions along the centerline (r = 0) to identify the textural components. As predicted, the rotated PFs in these regions can be interpreted as dominant $B/\overline{B}$, weak $A_1^*/A_2^*$ and C simple-shear texture, as depicted in PFs and ODFs in Figs. 13 and 14, respectively.

After passing the TMAZ 1, the material is extruded into the die orifice, forming a wire. The textural data does not change along the centerline of the wire (regions r40 and r50), while the PFs rotated CCW in regions r41 and r51, as seen in Fig. 12. Region r5m has completely different texture components compared to other regions. As observed in Fig. 3b, there is no visible pattern on the wire surface induced by a rotating die in radial direction. Therefore, it suggests that the material flow in this region is mainly determined by shear strain induced by extrusion in longitudinal direction [21]. However, texture development in the region r5m is not well understood. Nevertheless, formation of the new grain orientation near <100> (Fig. 10) might be associated with the <100> recrystallization texture [4].

Fig. 15 presents the 111 and 110 PFs extracted near the transition region in samples III and VI, i.e. from the Region 4 according to Fig. 6. Both regions have strong crystallographic orientation of <110> parallel to TD. The as-acquired 111 PFs show similar texture components with strong intensity near the upper and lower poles, however, there is a deviation from the vertical line, i.e. the intensity peaks rotate CCW and clockwise in samples III and VI, respectively. To a first approximation, the material flow is characterized by SP aligned with the flow line or macroscopic boundary between the BM and TMAZ [19]. Rearrangement of the as-acquired PFs to align SPN horizontally and SD vertically reveals that $B/\overline{B}$ is the predominant shear texture components with $A_1^*/A_2^*$and C present to a lesser extent, as presented in the PFs and ODFs.

Fonda and Bingert [35] showed that the $A_1^*/A_2^*$ and C simple shear texture components predominate at low strains during FSW, which then will be gradually replaced by $B/\overline{B}$ texture components at higher strains. Presence of strong $B/\overline{B}$ with minor $A_1^*/A_2^*$ and C in this study indicates that the material appears to have been subjected to large strains in TMAZ 1 during the FE process. Formation of the different texture components in various regions is mainly associated with the local strain. Based on the textural data, shear deformation during FE is characterized as simple shear with mainly two different shear-plane alignments, perpendicular and along ED, in addition to die-face-induced shear strain. The shear-plane perpendicular to ED is mainly driven by the radial movement of the tool, i.e. die face, which is also known as in-plane shear strain [4].

## 5. Material flow during friction extrusion

Alignment of the SPs varies in the TMAZ 1 and wire depending on their locations. Based on the microstructure and textural data for FE with extrusion force large than 19 kN, the proposed material flow during FE to produce a homogenous fine-grained microstructure is presented in Fig. 16.

In the beginning of the FE process, the die introduces severe plastic deformation and generates frictional heat that softens the imminent materials with SP and SD aligned with the die face and rotation direction, respectively. Next, the material at the die-material interface sticks to the rotating die and accelerates when the friction shear stress exceeds the material's yield stress [36]. Then the material moves with the same radial velocity as the rotating die. After that, the softened material flows

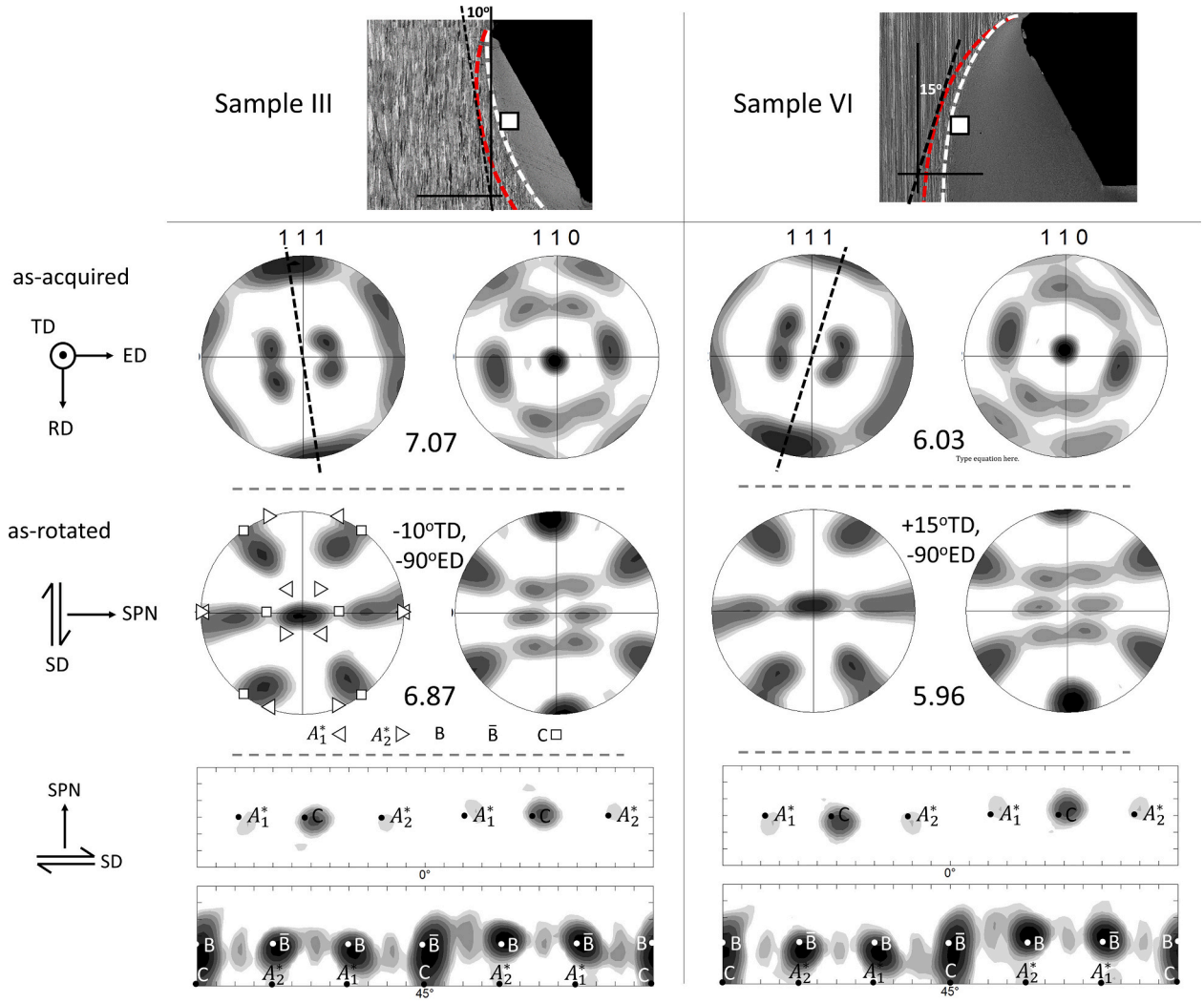


**Fig. 15.** Crystallographic maps derived from the transition region (Region 4, which belongs to TMAZ 1, see Fig. 6) in samples III and VI.

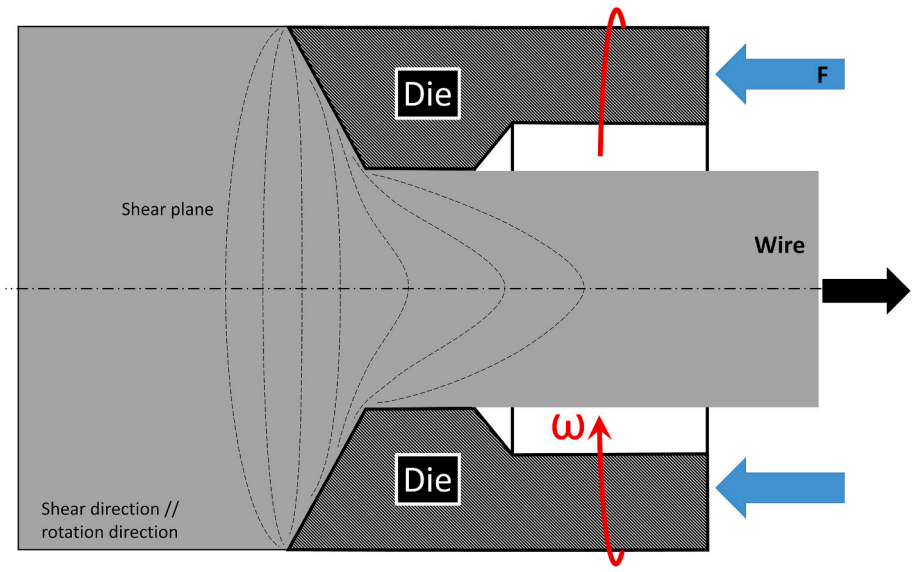


**Fig. 16.** Proposed material flow during the FE process to produce homogeneous fine-grained wire. Dash lines represent the shear planes with shear direction aligned to the rotation direction.

towards the die orifice, as depicted in samples I-V in Fig. 5. Accumulation of the softened material at the die orifice slows down the extrusion rate [3]. Suitable combination of the die-face-induced strain and extrusion-induced strain at elevated temperature leads to formation and extension of the in-plane shear strain towards the BM. The in-plane strain deforms the material with SP perpendicular to ED, as presented in Fig. 13. At the same time, the fine-grained area extends towards the BM, reaching the equilibrium volume, as observed in Sample VI in Fig. 5. Finally, the extrusion-induced strain forces the material through the die orifice, resulting in a homogeneous fine-grained wire. Sticking of the material to the die can be observed from the surface appearance of the extruded wire (Fig. 3b), indicating that the relative rotation between the rotating die and the wire is (nearly) zero. Based on the material flow prediction, it is likely that the in-plane and extrusion-induced strains are more pronounced with the radius increment, as can also be observed by texture intensity (Imax), in Figs. 12 and 13. Additionally, the extrusion-induced strain increases towards the die orifice due to the die diameter reduction [4]. It is also important to note that the flowing mechanism of the material in the ED seems to be layer by layer continuously, in which the first layer is pushed towards the die orifice by the following layer. Formation and development of the materials in the transition zone in this manner are beneficial for the production of a homogeneous fine-grained microstructure within the wire.

Meanwhile, microstructure development in the wires produced by the extrusion force <19 kN, leading to an inhomogeneous microstructure, are explained in the following. The wires consist of fine-grained structure of TMAZ 1 in the area along the die face and elongated grains in a larger TMAZ 2, as presented in Fig. 3a. Additionally, the wire surface exhibits an obvious pattern because of deformation induced by die rotation. This observation indicates that the relative rotation between the rotating die and the wire is relatively large, i.e. sliding. The sliding condition occurs when the contact shear stress is smaller than the material yield shear stress [36,37]. Therefore, the rotating die shears only a limited material near the die face. The result suggests that a combination of the die rotation speed and the extrusion force was not suitable for generating sufficient in-plane shear strain, which is mainly responsible for the formation and development of a homogeneous fine-grained area or the TMAZ 1.

## 6. Conclusions

In the present study, the microstructure evolution and texture development during friction extrusion were investigated via in-depth microstructural and texture analyses. The main conclusions are as follows:

1. Based on grain characteristic, the microstructure in the transition material, i.e. in front of the die orifice, is divided into the thermo-mechanically affected zone (TMAZ) 1 that comprises a fine-grained structure and the TMAZ 2 that consists of a deformed grain structure, in addition to the base material.
2. Continuous dynamic recrystallization (CDRX) induced by grain subdivision and lattice rotation and geometric dynamic recystallization (GDRX) induced by geometrical effect of strain seem to have great contribution to the global grain refinement during FE of AA7075 with a limited discontinuous dynamic recrystallization (DDRX) induced by grain boundary bulging. It should be noted that transition from the CDRX to GDRX and DDRX is observed at elevated temperature.
3. The shear deformation during friction extrusion was characterized as a simple shear with different alignments of the shear plane to the die face, perpendicular to extrusion direction and die orifice. The developed texture was interpreted as dominant $B/\overline{B}$, weak $A_1^*/A_2^*$ and C simple-shear texture.
4. A material flow model for FE is proposed during fabrication of the homogeneous fine-grained wire. The material flow is mainly driven by the in-plane shear strain acting perpendicular to extrusion direction (ED) and extrusion-induced shear strain along the ED. Under sticking condition, the material flow occurs layer by layer.
5. Development of the in-plane shear strain is strongly affected by die-face-induced shear strain associated with the tool rotation speed and the extrusion-induced shear strain associated with the extrusion force. Absence of the in-plane shear strain leads to formation of inhomogeneous microstructure due to slipping condition, which is broadly similar to the conventional extrusion process.

## Declaration of Competing Interest

None.

## Data availability

The data related to this research will be published online under https://doi.org/10.5281/zenodo.7965677.

## Acknowledgments

This project has received funding from the European Research Council (ERC) under the European Union's Horizon 2020 Research and Innovation Programme (grant agreement No 101001567).

## References

[1] D. Baffari, A.P. Reynolds, X. Li, L. Fratini, Influence of processing parameters and initial temper on friction stir extrusion of 2050 aluminum alloy, J. Manuf. Process. 28 (2017) 319–325, https://doi.org/10.1016/j.jmapro.2017.06.013.
[2] R. Kalsar, X. Ma, J. Darsell, D. Zhang, K. Kappagantula, D.R. Herling, V.V. Joshi, Microstructure evolution, enhanced aging kinetics, and mechanical properties of AA7075 alloy after friction extrusion, Mater. Sci. Eng. A 833 (2022), 142575, https://doi.org/10.1016/j.msea.2021.142575.
[3] R.M. Halak, L. Rath, U.F.H.R. Suhuddin, J.F. dos Santos, B. Klusemann, Changes in processing characteristics and microstructural evolution during friction extrusion of aluminum, Int. J. Mater. Form. 15 (2022) 24, https://doi.org/10.1007/s12289-022-01670-y.
[4] X. Li, W. Tang, A.P. Reynolds, W.A. Tayon, C.A. Brice, Strain and texture in friction extrusion of aluminum wire, J. Mater. Process. Technol. 229 (2016) 191–198, https://doi.org/10.1016/j.jmatprotec.2015.09.012.
[5] D. Baffari, G. Buffa, D. Campanella, L. Fratini, A.P. Reynolds, Process mechanics in friction stir extrusion of magnesium alloys chips through experiments and numerical simulation, J. Manuf. Process. 29 (2017) 41–49, https://doi.org/10.1016/j.jmapro.2017.07.010.
[6] W. Tang, A.P. Reynolds, Production of wire via friction extrusion of aluminum alloy machining chips, J. Mater. Process. Technol. 210 (2010) 2231–2237, https://doi.org/10.1016/j.jmatprotec.2010.08.010.
[7] R.A. Behnagh, R. Mahdavinejad, A. Yavari, M. Abdollahi, M. Narvan, Production of wire from AA7277 aluminum chips via friction-stir extrusion (FSE), Metall. Mater. Trans. B Process Metall. Mater. Process. Sci. 45 (2014) 1484–1489, https://doi.org/10.1007/s11663-014-0067-2.
[8] S. Whalen, M. Olszta, C. Roach, J. Darsell, D. Graff, M. Reza-E-Rabby, T. Roosendaal, W. Daye, T. Pelletiers, S. Mathaudhu, N. Overman, High ductility aluminum alloy made from powder by friction extrusion, Materialia. 6 (2019), https://doi.org/10.1016/j.mtla.2019.100260.
[9] S. Whalen, N. Overman, V. Joshi, T. Varga, D. Graff, C. Lavender, Magnesium alloy ZK60 tubing made by shear assisted processing and extrusion (ShAPE), Mater. Sci. Eng. A 755 (2019) 278–288, https://doi.org/10.1016/j.msea.2019.04.013.
[10] X. Li, C. Zhou, N. Overman, X. Ma, N. Canfield, K. Kappagantula, J. Schroth, G. Grant, Copper carbon composite wire with a uniform carbon dispersion made by friction extrusion, J. Manuf. Process. 65 (2021) 397–406, https://doi.org/10.1016/j.jmapro.2021.03.055.
[11] Y. Hosseini, A. Hosseini, E. Azarsa, B. Davoodi, Ardahani, Effect of process parameters on the physical properties of wires produced by friction extrusion method, Int. J. Adv. Eng. Technol. 3 (2012) 592–597.
[12] G. Buffa, D. Campanella, L. Fratini, F. Micari, AZ31 magnesium alloy recycling through friction stir extrusion process, Int. J. Mater. Form. 9 (2015) 613–618, https://doi.org/10.1007/s12289-015-1247-6.
[13] A.K. Lakshminarayanan, K.S. Jayakumar, Use of friction extrusion to fabricate magnesium alloy wires with rare Earths from machined chips, Mater. Sci. Forum 979 (2020) 119–123, https://doi.org/10.4028/www.scientific.net/MSF.979.119.
[14] T. Wang, J.E. Atehortua, M. Song, M. Reza-E-Rabby, B.S. Taysom, J. Silverstein, T. Roosendaal, D. Herling, S. Whalen, Extrusion of Unhomogenized castings of

7075 aluminum via ShAPE, Mater. Des. 213 (2022), 110374, https://doi.org/10.1016/j.matdes.2021.110374.
[15] A.P. Li, X.W. Tang, X. Li Reynolds, W. Tang, A.P. Reynolds, Material flow and texture in friction extruded wire, in: Frict. Stir Weld. Process. VII, John Wiley & Sons, Inc., 2013, pp. 339–347, https://doi.org/10.1002/9781118658345.ch35.
[16] T. Sakai, A. Belyakov, R. Kaibyshev, H. Miura, J.J. Jonas, Dynamic and post-dynamic recrystallization under hot, cold and severe plastic deformation conditions, Prog. Mater. Sci. 60 (2014) 130–207, https://doi.org/10.1016/j.pmatsci.2013.09.002.
[17] J. Lv, J.-H. Zheng, V.A. Yardley, Z. Shi, J. Lin, A review of microstructural evolution and modelling of Aluminium alloys under hot forming conditions, Metals (Basel). 10 (2020) 1516, https://doi.org/10.3390/met10111516.
[18] T. Sakai, H. Miura, A. Goloborodko, O. Sitdikov, Continuous dynamic recrystallization during the transient severe deformation of aluminum alloy 7475, Acta Mater. 57 (2009) 153–162, https://doi.org/10.1016/j.actamat.2008.09.001.
[19] P.B. Prangnell, C.P. Heason, Grain structure formation during friction stir welding observed by the 'stop action technique,', Acta Mater. 53 (2005) 3179–3192, https://doi.org/10.1016/j.actamat.2005.03.044.
[20] J.-Q. Su, T.W. Nelson, C.J. Sterling, Microstructure evolution during FSW/FSP of high strength aluminum alloys, Mater. Sci. Eng. A 405 (2005) 277–286, https://doi.org/10.1016/j.msea.2005.06.009.
[21] A. Güzel, A. Jäger, F. Parvizian, H.-G. Lambers, A.E. Tekkaya, B. Svendsen, H. J. Maier, A new method for determining dynamic grain structure evolution during hot aluminum extrusion, J. Mater. Process. Technol. 212 (2012) 323–330, https://doi.org/10.1016/j.jmatprotec.2011.09.018.
[22] W. Blum, Q. Zhu, R. Merkel, H.J. McQueen, Geometric dynamic recrystallization in hot torsion of Al-5Mg-0.6Mn (AA5083), Mater. Sci. Eng. A 205 (1996) 23–30, https://doi.org/10.1016/0921-5093(95)09990-5.
[23] S. Mironov, K. Inagaki, Y.S. Sato, H. Kokawa, Effect of welding temperature on microstructure of friction-stir welded aluminum alloy 1050, Metall. Mater. Trans. A. 46 (2015) 783–790, https://doi.org/10.1007/s11661-014-2651-0.
[24] F.J. Humphreys, M. Hatherly, Chapter 13 - Hot Deformation and Dynamic Restoration, in: F.J. Humphreys, M.B.T.-R. and R.A.P. Second E. Hatherly (Eds.), Elsevier, Oxford, 2004, https://doi.org/10.1016/B978-008044164-1/50017-7, 415–V.
[25] U. Suhuddin, S. Mironov, H. Krohn, M. Beyer, J. Dos Santos, Microstructural evolution during friction surfacing of dissimilar aluminum alloys, Metall. Mater. Trans. A. (2023) 1–8, https://doi.org/10.1007/s11661-012-1345-8.
[26] S. Mironov, Y.S. Sato, H. Kokawa, Grain structure evolution during friction-stir welding, Phys. Mesomech. 23 (2020) 21–31, https://doi.org/10.1134/S1029959920010038.
[27] J.-Q. Su, T.W. Nelson, C.J. Sterling, Grain refinement of aluminum alloys by friction stir processing, Philos. Mag. 86 (2006) 1–24, https://doi.org/10.1080/14786430500267745.
[28] X. Xu, Y. Zhao, X. Wang, Y. Zhang, Y. Ning, The rapid age strengthening induced by ag additions in 7075 aluminum alloy, Mater. Sci. Eng. A 648 (2015) 367–370, https://doi.org/10.1016/j.msea.2015.09.044.
[29] J. Zhao, Y. Deng, J. Tan, J. Zhang, Effect of strain rate on the recrystallization mechanism during isothermal compression in 7050 aluminum alloy, Mater. Sci. Eng. A 734 (2018) 120–128, https://doi.org/10.1016/j.msea.2018.07.068.
[30] B. Liao, X. Wu, L. Cao, G. Huang, Z. Wang, Q. Liu, The microstructural evolution of aluminum alloy 7055 manufactured by hot thermo-mechanical process, J. Alloys Compd. 796 (2019) 103–110, https://doi.org/10.1016/j.jallcom.2019.05.054.
[31] J. Shen, S.B.M. Lage, U.F.H. Suhuddin, C. Bolfarini, J.F. dos Santos, Texture development and material flow behavior during refill friction stir spot welding of AlMgSc, Metall. Mater. Trans. A Phys. Metall. Mater. Sci. 49 (2018) 241–254, https://doi.org/10.1007/s11661-017-4381-6.
[32] C. Xu, H. He, Z. Xue, L. Li, A detailed investigation on the grain structure evolution of AA7005 aluminum alloy during hot deformation, Mater. Charact. 171 (2021), 110801, https://doi.org/10.1016/j.matchar.2020.110801.
[33] H. Azzeddine, D. Bradai, T. Baudin, T.G. Langdon, Texture evolution in high-pressure torsion processing, Prog. Mater. Sci. 125 (2022), https://doi.org/10.1016/j.pmatsci.2021.100886.
[34] J. Li, J. Xu, C.T. Wang, D. Shan, B. Guo, T.G. Langdon, Microstructural evolution and micro-compression in high-purity copper processed by high-pressure torsion, Adv. Eng. Mater. 18 (2016) 241–250, https://doi.org/10.1002/adem.201500488.
[35] R.W. Fonda, J.F. Bingert, Texture variations in an aluminum friction stir weld, Scr. Mater. 57 (2007) 1052–1055, https://doi.org/10.1016/j.scriptamat.2007.06.068.
[36] H. Schmidt, J. Hattel, J. Wert, An analytical model for the heat generation in friction stir welding, Model. Simul. Mater. Sci. Eng. 12 (2003) 143–157, https://doi.org/10.1088/0965-0393/12/1/013.
[37] H.R. Doude, J.A. Schneider, A.C. Nunes, Influence of the tool shoulder contact conditions on the material flow during friction stir welding, Metall. Mater. Trans. A. 45 (2014) 4411–4422, https://doi.org/10.1007/s11661-014-2384-0.